Journal of Materials Science: Materials in Electronics (2019) 30:20198–20204
https://doi.org/10.1007/s10854-019-02403-9

Contrasting effects of metal oxide dopants on the superconductivity of $YBa_2Cu_3O_{7-\delta}$ ceramics

Murat Ozabaci[1]

Received: 22 August 2019 / Accepted: 16 October 2019 / Published online: 23 October 2019

Abstract
Bulk superconductor samples of $YBa_2Cu_3O_{7-\delta}$ (YBCO or Y-123), with additions of 0.15 wt% MoO_3, TiO_2, RuO_2 and two different types of Al_2O_3 compounds, are synthesized by a solid state reaction route. Structural, magnetic and transport properties of the samples are characterized using X-ray diffraction (XRD), scanning electron microscopy (SEM), energy dispersive X-ray analysis (EDX), magnetic (*M-H*, *M-T*) and magneto-resistivity (*MR-T*) measurements. SEM investigations show that the addition of the Al_2O_3 obtained from the alumina crucible (Al_2O_3-cru) decreases the grain size of the sample which, in turn, degrades the transition temperatures (T_c) and magnetic critical current densities (J_c^{mag}). On the contrary, the addition of the other metal oxides enhances J_c^{mag} of the samples by a few times and also increases T_c by up to 3 K. EDX analyses of the samples exhibit homogeneous distribution of additions, except for Ru-heterogeneities located around superconducting Y-123 grains. The highest J_c and T_c values obtained on the RuO_2 added sample were attributed to the agglomeration of the Ru-particles, which led to the optimal porosity that supports oxygenation process and intergrain coupling of the structure. From the DC magnetization data, we estimated J_c^{mag} of 3.1×10^5 A/cm^2, 2.3×10^5 A/cm^2, 2×10^5 A/cm^2, 1.5×10^5 A/cm^2, 10^5 A/cm^2 and 5.1×10^4 A/cm^2 for the RuO_2, TiO_2, MoO_3, Al_2O_3, undoped and Al_2O_3-cru added samples at 5 K under 0.25 T, respectively.

1 Introduction

Since the discovery of high temperature superconductivity (HTSCs) in layered Y–Ba–Cu–O (YBCO) ceramics in 1986, a huge effort has been made to improve its superconducting properties [1]. For many engineering applications, such as electric power transmission systems, magnetic bearings, trapped flux magnet etc., high transition temperature (T_c), narrow transition width (ΔT) and high critical current density (J_c) are desired [2–4]. However, the effect of weak links between superconducting grains and the weak pinning of flux lines are the main limitations of these materials for technological applications. Substituting constitutional elements and creating defects are popular methods to overcome these obstacles, as they produce artificial pinning centers [5, 6]. Pr, Sm, Al, La, Yb, graphene, Ag, C, Fe, Ni, Ba, Ti, Sr, Zn, Co, Cu, Au and Lu are examples of additions and substitutions that have already been performed to the YBCO using various techniques [7–17].

In these studies, it has been found that the addition of secondary particles in some cases enhances electrical stability, magnetic flux trapping, mechanical properties, grain orientation and grain growth, as well as T_c and J_c, and reduces the normal-state resistivity (ρ_n). It has been shown that it is very important to control the size, volume and distribution of added particles to improve the critical current density up to 10^5–10^7 A/cm^2 under 20 K [18–20]. Besides, electron, neutron or heavy ion irradiation led to remarkable progress in achieving high J_c's by creating crystal lattice distortions [21, 22].

It is known that electronic properties and crystalline structure of YBCO are strongly governed by the amount of oxygen in Y-123. Therefore, among the different compounds used as dopants, metal oxides were mostly studied in the literature to avoid additional oxygen vacancies that are likely to degrade the transition temperature of the samples.

The aim of this study is to investigate the microstructure and physical properties of $Y_1Ba_2Cu_3O_{7-\delta}$ (Y-123) + 0.15 wt% Al_2O_3 (obtained from two different sources), MoO_3, TiO_2, RuO_2 polycrystalline samples. We aimed to introduce

✉ Murat Ozabaci
muratozabaci@yahoo.com

[1] Scientific and Technological Research Center, SEM/EDX Lab. Inonu University, Malatya, Turkey

additional pinning centers and depress the infield negative effects on J_c stemming from flux creep. The samples were prepared by employing the classical solid state reaction technique and characterized using scanning electron microscope, X-ray diffraction, transport and magnetic measurements.

2 Experimental

Solid state reaction was used in preparing $Y_1Ba_2Cu_3O_{7-\delta}$ (Y-123) samples with separately added 0.15 wt% Al_2O_3-cru (obtained through intermediate grinding of alumina substrate, Sigma-Aldrich, 99.8%, hereafter will be denoted as Al_2O_3-cru), Al_2O_3 (Alfa Aesar, 99.9%),, MoO_3 (Aldrich, 99.5+ %), TiO_2 (Alfa Aesar, 99.9%) and RuO_2 (Alfa Aesar, 99.9%). Stoichiometric proportions of thoroughly mixed Y_2O_3 (Reacton, 99.9%), $BaCO_3$ (Aldrich, 99+ %), CuO (Alfa Aesar, 99.7%) and separately added Al_2O_3-cru, Al_2O_3, MoO_3, TiO_2 and RuO_2 were calcinated for 24 h at 880 °C and 900 °C with two intermediate grindings. After calcination, the powders were pressed into pellets of 2 mm thickness and 13 mm diameter at 400 MPa. The final pellets were annealed at 980 °C for 24 h and then cooled to 480 °C where these were kept for 4 h, in a flowing oxygen atmosphere, before slowly cooling to room temperature.

Phase analysis of all samples was performed by powder X-ray diffraction (XRD) utilizing a Rigaku Miniflex 600 diffractometer with Cu-Kα (40 kV, 15 mA, λ = 1.54050 Å) radiation over the range 2θ = 10–80° at room temperature at a scan rate of 3°/min. Morphological and elemental properties were observed using LEO EVO-40 scanning electron microscope (SEM) attached with a Bruker energy dispersive X-ray spectrometer (EDX). The electrical resistivity was measured as a function of temperature (*R-T*) between 30 and 150 K in self-field and under DC magnetic fields of 2 and 4 T using the conventional four probe configuration. 1 mA AC (17 Hz) current was applied during *R-T* measurements. Transport and DC magnetization measurements (*R-T, MR-T, M-T* and *M-H*) were carried out in a Quantum Design Physical Properties Measurement System (PPMS-9 T). The critical current densities were calculated from the magnetic hysteresis loops (*M-H*) measured at 5, 15 and 25 K up to 8 T via the extended Bean critical state model formula. The zero-field-cooled (ZFC) mode was applied under 100 Oe in the range 5–150 K to evaluate the magnetic transition temperatures through the *M-T* curves.

3 Results and discussion

Figure 1 shows the powder X-ray diffraction patterns and corresponding (*hkl*) Miller indices of the undoped and slightly doped YBCO samples. It is obvious that all the

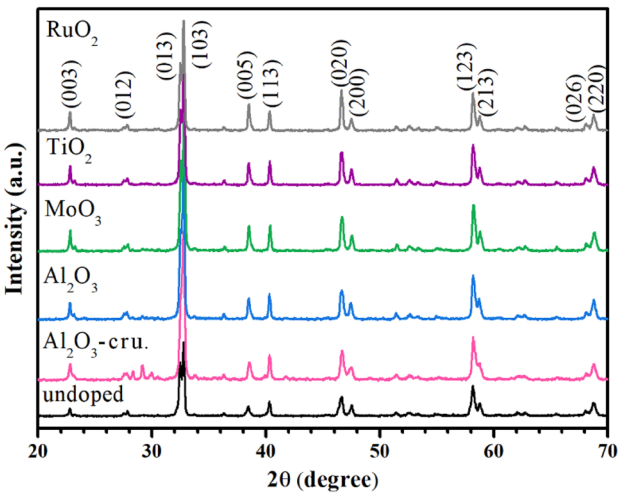

Fig. 1 XRD patterns of pure and 0.15 wt% doped $Y_1Ba_2Cu_3O_{7-\delta}$ samples

main XRD peaks of the pure and doped samples belong to orthorhombic phase of Y-123. The patterns show the characteristic polycrystalline structure of the Y-123 compound. The absence of additional phases in the pattern, such as Y_2BaCuO_5, $BaCuO_2$, $BaCO_3$ and Y_2O_3, shows the high purity of the samples. In all the obtained patterns, the peaks caused by additions are indistinguishable, which is connected with their minor amount in the samples. The relative intensity, width, sharpness and positions of the peaks do not show significant difference depending on the dopants. This means that 0.15 wt% addition does not have much influence on the phase formation and crystallographic structure of Y-123.

Surface morphologies of the samples were studied by SEM in order to observe the shape, size and orientation of the grains, porosity and possible precipitations of the doped elements. The grains of Y-123 have an irregular shape with no specific alignment in the range of 1-15 μm, as shown in Fig. 2.a–f. There is only a small number of round pores between the closely packed grains. It is evident in Fig. 2b that the addition of Al_2O_3-cru seriously degrades the grain sizes, as well as grain connectivity. The images in Fig. 2c–e, present the characteristic layered growth of the Y-123 along with rectangular-like grains, suggesting that two-dimensional growth is energetically more favorable. It is observed that the addition of 4 other metal oxides facilitates the grain growth and partly fills in pores and micro-cracks. On the other hand, it has been observed on the Ru-doped sample in Fig. 2f that RuO_2 is not totally incorporated into the host matrix. This suggests that solid solubility of RuO_2 in the Y-123 is lower than the 0.15 wt% doping amount. The presence of Ru particles was also verified by EDX elemental mapping analysis as given in Fig. 3a, b. EDX measurements

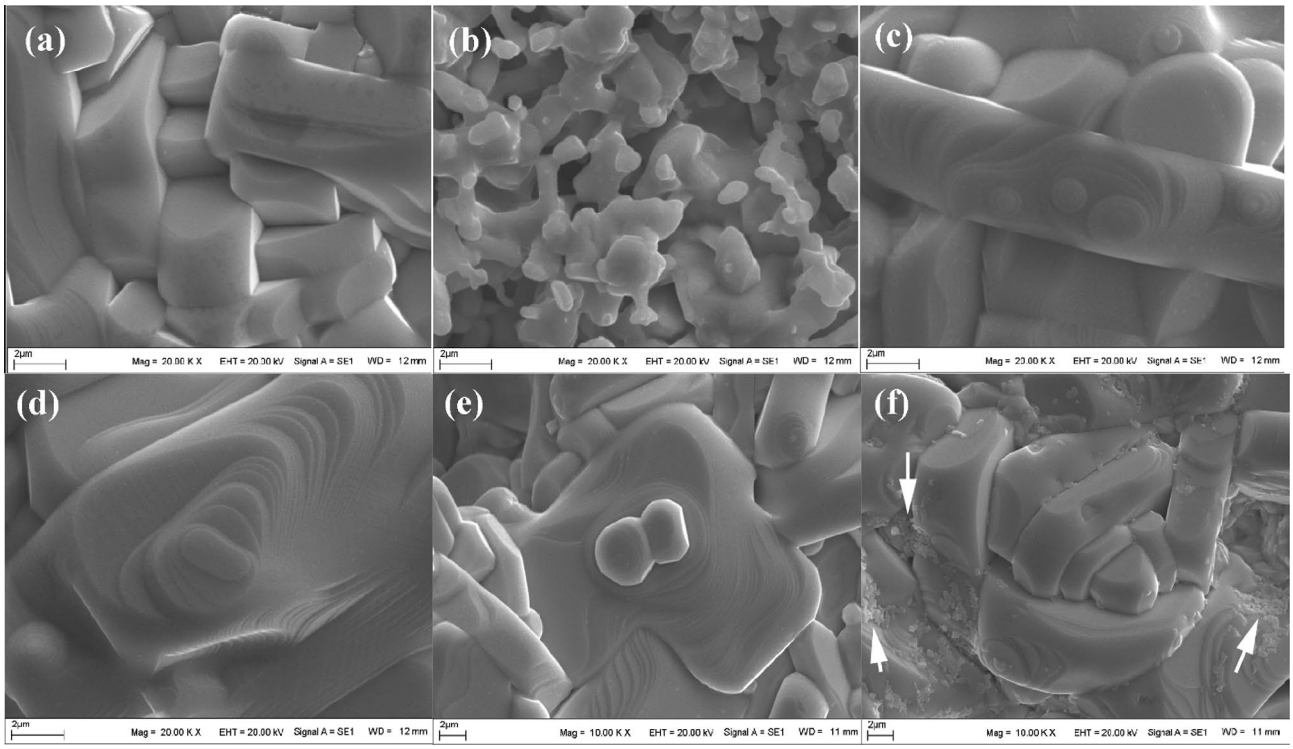

Fig. 2 SEM microstructures of the bulk Y-123 with additives: **a** undoped, **b** Al_2O_3-cru, **c** Al_2O_3, **d** MoO_3, **e** TiO_2, **f** RuO_2. Arrows indicate the Ru precipitation regions

confirmed the Y-123 stoichiometry, while elemental mappings showed the homogeneity of all the samples except for the Ru heterogeneities dispersed in the matrices. However, the signals stemming from the Al, Mo, and Ti could not be detected on the EDX spectra, which is attributed to the amount of doping that is below EDX detection limit.

Transition temperature, T_c^{mag}, values were determined from the onset of diamagnetic signal in DC magnetization versus temperature curves obtained at 5–140 K, Fig. 4. T_c^{mag} values were found to be around 91.5 K for the samples, suggesting that the presence of the additions does not degrade the critical superconducting parameters of the Y-123, Table 1. However, saturation magnetization levels show differences depending on added compositions. Al_2O_3-cru addition significantly decreases the diamagnetic signal level, while this decrease is slight for Al_2O_3addition. On the other hand, the additions of MoO_3, TiO_2 and RuO_2 increase the saturation magnetization level, more pronouncedly for the RuO_2 addition, as shown in Fig. 4. The large Meissner signal indicates that it has good bulk superconductivity.

Figure 5a–c presents the *M-H* curves of the samples obtained at three different temperatures 5 K, 15 K and 25 K. *M-H* curves show the symmetrical behavior, which is a characteristic of type-II superconductors. The central maximum magnetization level observed in zero applied field is the highest for RuO_2-added sample and it decreases continuously with additions of TiO_2, MoO_3, undoped, Al_2O_3 and Al_2O_3-cru, respectively. Critical current densities of the samples, J_c^{mag}, were calculated by using Bean's critical state model, with the formula, $J_c^{mag} = \frac{20\Delta M}{a(1-a/3b)}$, in the field range of 0–8 T [23, 24]. In this formula, ΔM is the width of the magnetization loop in emu/cm^3, a and b ($b > a$) are the in-plane dimensions of the samples. All the J_c^{mag} curves follow exponential T dependence at 5 K. The calculated results shown in Fig. 5d–f and Table 2 demonstrate that the highest value of J_c^{mag} of 3.1×10^5 A/cm^2 is reached in the RuO_2-added sample at 5 K under 2.5 kOe and then decreases to $J_c^{mag} = 2.3 \times 10^5$ A/cm^2, 2×10^5 A/cm^2 and 1.5×10^5 A/cm^2 for the TiO_2, MoO_3 and Al_2O_3 added samples under same conditions, respectively. These values are a few times larger than that of the undoped sample, showing the enhancement of the pinning capability of samples through a possible increase in the number of microscale crystal defects. Furthermore, the addition of RuO_2, TiO_2 and MoO_3 could enhance the metallic character of nanoscale secondary phases at grain boundaries, thus improving grain connectivity and intergrain coupling. On the other hand, it can be said that the addition of Al_2O_3-cru does not involve chemical pinning, and thus drops the J_c^{mag} as low as 5.1×10^4 A/cm^2 which is almost half of the undoped one. The order of curves does not

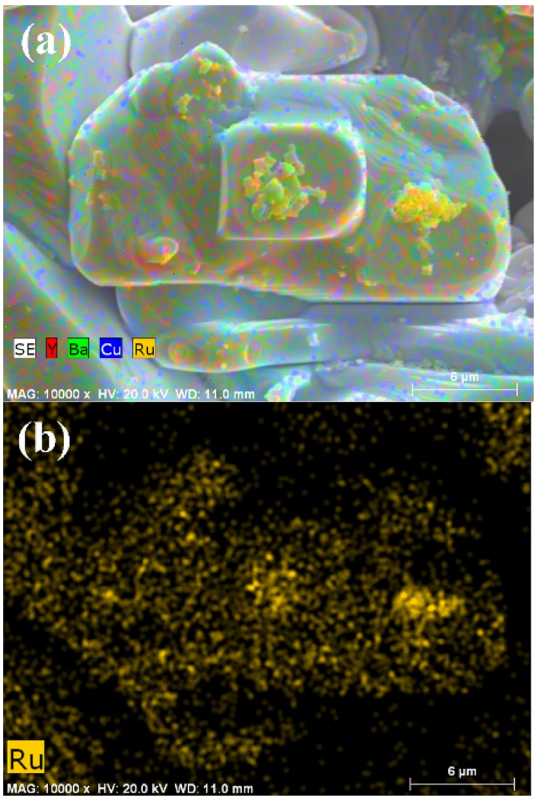

Fig. 3 EDX elemental mapping images of **a** RuO_2 added Y-123 and **b** single Ru element (Y is shown in red, Ba in green, Cu in blue and Ru in yellow) (Color figure online)

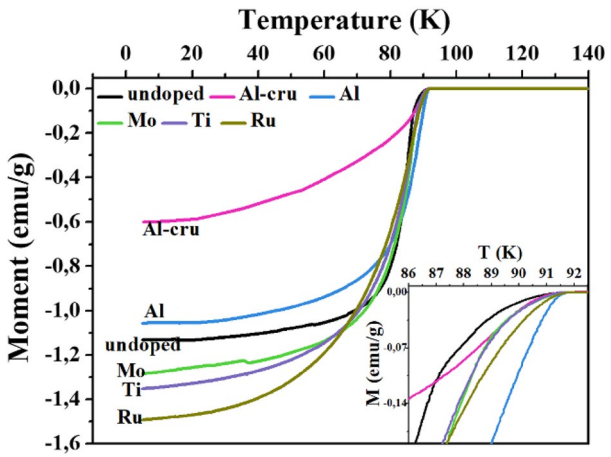

Fig. 4 Magnetization versus temperature plots of the samples. Inset shows the expanded view in the normal-to-superconducting transition region

change for the measurements realized at 15 K and 25 K. However, the influence of applied magnetic field on J_c^{mag} weakens especially at magnetic fields higher than 3 T for the 15 K and 25 K measurements.

The temperature-dependent resistivity measurements of the samples were performed under applied fields up to 4 T. All samples show metallic behavior above T_c^{onset} values. The appearance of zero-resistance state within a narrow temperature range, i.e. $\Delta T = 1$–4 K, shows compact crystal structure of the samples. It is clear from Fig. 6a–c that both the increase of magnetic field, up to 4 T, and various additions weakly affect the onset of superconductivity. T_c^{onset} values were found to be in the range of 90–91.3 K for all the compositions under self-field, 2 T and 4 T, Table 1. However, increased magnetic field and different additions broaden the transition by decreasing the T_c^{zero} values from around 87–89 K to around 68–81 K. The appearance of resistive tails on the lower temperature end of *R-T* curves is related with an energy dissipation mechanism stemming from motion of fluxons by Lorentz force and thermal energy. This is known as thermally activated flux flow (TAFF) [25]. The most significant decrease was observed on Al_2O_3-cru added sample with an increase of $\Delta T = 20$ K from $T_c^{zero} = 87.9$ K (0 T) to $T_c^{zero} = 68.1$ K (4 Tesla). This decrease was only around 8 K, from $T_c^{zero} = 89.1$ K (0 T) to $T_c^{zero} = 81.2$ K for the RuO_2 added sample. It seems that the only dopant lowering the normal state resistivity of the samples is RuO_2 while Al_2O_3-cru doping leads to the highest normal state resistivity. RuO_2 doping also increases the T_c^{zero} values a few kelvin. Since the added RuO_2 is not completely dissolved in Y-123, as observed in SEM images, it is suggested that Ru atoms do not substitute the major components of the Y-123 and adhere to grain boundary forming weak links. This behavior can also promote the oxygenation of the Y-123 superconducting grains by leading optimal porosity. Hence, RuO_2 doping might support reaching of optimal values in hole carrier concentration in the superconducting phase of the Y-123.

The strongest influence of external magnetic field on resistive transition is obtained for the Al_2O_3-cru doped sample, which is attributed to the smaller grains and larger number of grain boundaries as observed in SEM investigations. It is evaluated that, in contrast to the other metal oxide additions, the addition Al_2O_3-cru increases the peritectic temperature of the YBCO which obstructs chemical interaction of the doped atoms with the host matrix. The presence of these unreacted powders during annealing contributes to the nucleation of additional Y-123 grains and creates more grain boundaries. The decrement observed on J_c values, in the case of Al_2O_3-cru addition, is ascribed to increasing numbers of grain boundaries which seem to act as resistance towards superconducting carriers. Furthermore, in addition to having two different fabrication routes, contrasting effects of Al_2O_3 and Al_2O_3-cru on the J_c^{mag} of the Y-123 could be related to the size of the doped powders, since the Al_2O_3-cru was obtained by manual grinding, the size of the doped powders are much larger (on the order of a few tens of µm) than that of commercial Al_2O_3 with mean size diameter

Table 1 Superconducting transition temperatures (in Kelvin) of the samples derived both from magneto-resistivity (*MR-T*) and magnetization measurements

Composition	*M-T*	*MR-T*											
		0 T				2 T				4 T			
	T_c^{mag}	T_c^{onset}	T_c^{zero}	ΔT	$T_c^{midpoint}$	T_c^{onset}	T_c^{zero}	ΔT	$T_c^{midpoint}$	T_c^{onset}	T_c^{zero}	ΔT	$T_c^{midpoint}$
Undoped	91.3	91	87	4	90.6	90.3	80.3	10	88.4	90	77.8	12.2	87.3
Al_2O_3-cru	91.3	90.9	87.9	3	90.2	91.1	71.5	19.6	89.2	91.3	68.1	23.2	88.6
Al_2O_3	91.6	90.9	89.3	1.6	90.4	90.8	77.4	13.4	89.6	90.8	74.5	16.3	89.2
MoO_3	91.5	90.9	87.9	3	90.3	90.3	81.6	8.7	88.4	91.1	78	13.1	87.7
TiO_2	91.4	90.8	88.1	2.7	90.2	90.8	82.6	8.2	88.5	90.8	77.2	13.6	87.4
RuO_2	91.6	91.1	89.1	2	90.4	90.6	83.1	7.5	89.2	90.8	81.2	9.6	88

$T_c^{midpoint}$ values inferred from the peak points of the dρ/dT curves

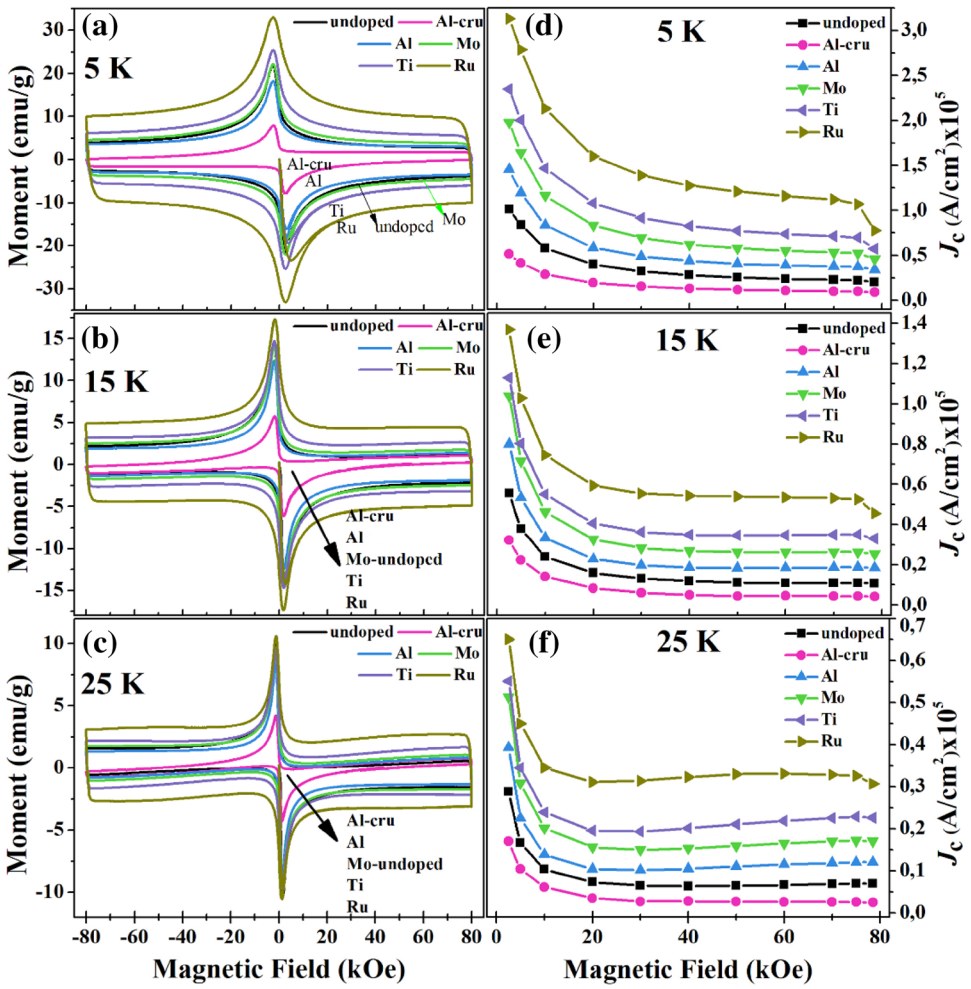

Fig. 5 **a–c** Magnetization versus magnetic field curves of the samples, **d-f** calculated magnetic critical current densities of the samples between 0 and 8 T at 5, 15, 25 K

of about 1 µm. On the other hand, compared to the ceramic phases, the mobility of the metal oxides are higher and therefore, addition of other metal oxide impurities, namely MoO_3, TiO_2 and RuO_2, facilitates grain growth and fills in microcracks, thus promoting T_c^{zero} and J_c^{mag} values in most cases.

These results are generally consistent with previously published data for Y-123 fabricated through different techniques. For example, in a study realized by Kim et al. using top-seeded melt growth process, it was found that low level Mo substitution to the Cu site (< 1 wt%) led to a small decrease of the T_c and increase of the J_c while high level substitutions caused a large J_c decrease [26]. The J_c enhancement by the low level Mo substitution was attributed to the Mo incorporation with the CuO chains as an

Table 2 Calculated magnetic critical current densities, J_c^{mag}, of the samples at 5 and 15 K

	J_c^{mag} (A/cm^2)×10^5											
Tempr.→	5 K						15 K					
Material→	Un-doped	Al_2O_3-cru	Al_2O_3	MoO_3	TiO_2	RuO_2	Un-doped	Al_2O_3-cru	Al_2O_3	MoO_3	TiO_2	RuO_2
Mag. field↓												
0.25 T	1.01	0.51	1.5	1.98	2.35	3.13	0.56	0.32	0.8	1.04	1.13	1.36
0.5 T	0.84	0.41	1.2	1.64	2.01	2.79	0.38	0.22	0.53	0.71	0.8	1.03
1 T	0.58	0.29	0.83	1.16	1.47	2.13	0.24	0.14	0.33	0.46	0.55	0.75
3 T	0.32	0.16	0.49	0.69	0.92	1.39	0.13	0.06	0.19	0.28	0.36	0.55
5 T	0.26	0.12	0.41	0.58	0.77	1.21	0.12	0.04	0.18	0.26	0.35	0.54
7 T	0.23	0.1	0.38	0.53	0.71	1.12	0.11	0.04	0.18	0.26	0.35	0.53
7.85 T	0.20	0.09	0.34	0.46	0.57	0.78	0.11	0.04	0.18	0.25	0.33	0.46

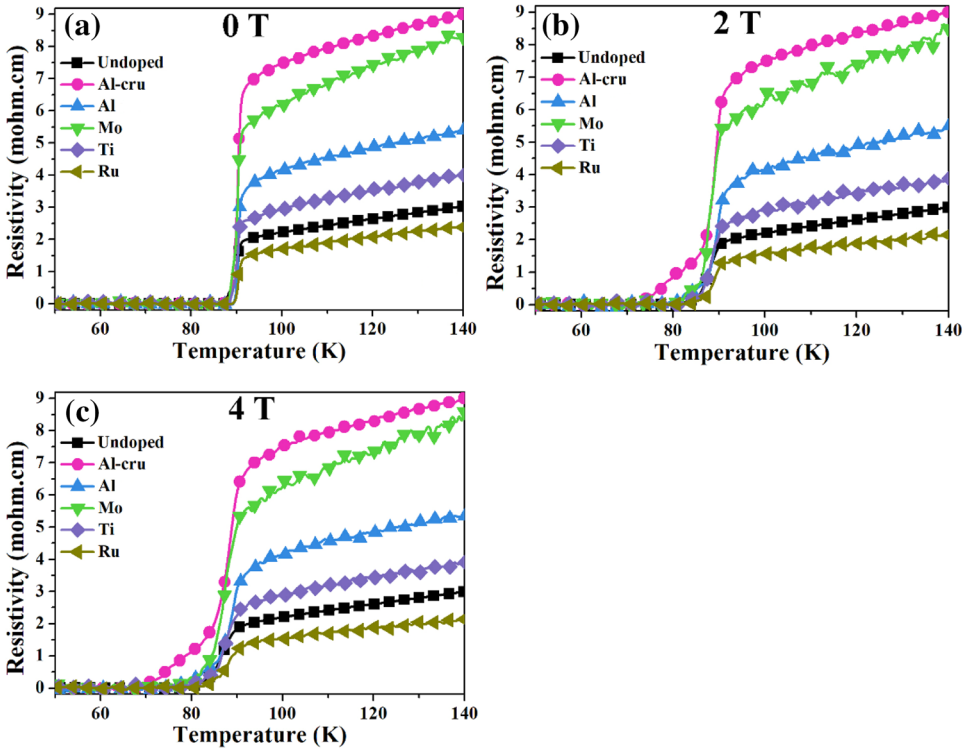

Fig. 6 Temperature-dependent resistivity of the samples under magnetic fields of **a** 0 T, **b** 2 T and **c** 4 T

extended point-like defects or nanoscale non-superconducting particles [27]. Yanmaz et al. researched TiO_2 doping effect in Y-123 by applying flame-quench-melt-growth (FQMG) method in weight percentages of 0, 1, 3, 5, 7 and 10 wt% [28]. They proposed that TiO_2 doping of Y-123 did not improve the weak-link behavior of the superconducting grains and the T_c. Since, the percentage of the added TiO_2 is higher than that of our study, it has been concluded that only minor amount of TiO_2 additions enhance the pinning properties of the Y-123. Krabbes et al. investigated the Ru doping (0.25–0.7 wt%) effect to melt-processed Y-123 bulk single grain samples and found that Ru is not dissolved in the Y-123 and forms the Y_2BaCuO_5 (Y-211) free Y-123 single crystal [29, 30]. They found flux-pinning weakening and lower J_c due to reduced contribution from Y-211 particles. Regarding our results obtained from the Ru added sample, the difference could be ascribed both to the different applied doping ranges and different crystalline forms. M'chirgui et al. embedded the insulating nano-Al_2O_3 particles with mean size diameters of about 130 nm and 150 nm into Y-123 and found that slight inclusions (< 0.1 wt%) can effectively enhance the flux pinning capability of samples without a change in T_c [31]. In connection with our results obtained from the Al_2O_3 and Al_2O_3-cru added samples, we

can deduce that as the size and amount of Al_2O_3 particles in the Y-123 decrease, the positive effects on the superconductivity increase.

4 Conclusion

The $YBa_2Cu_3O_{7-\delta}$ bulk superconductors with additions of 0.15 wt% Al_2O_3-cru, Al_2O_3, MoO_3, TiO_2 and RuO_2 were prepared by the conventional solid state reaction technique to investigate the effect of additions on the superconductivity of the Y-123. The XRD results showed single phase orthorhombic Y-123 for the whole range of impurities. SEM investigations revealed that the metal oxide additions improve the grain formation and grain connectivity, while Al_2O_3-cru lowers the size and connectivity of the grains leading to adverse effects on the J_c of the samples. EDX measurements confirmed the homogeneous distribution of doped elements except for Ru precipitates located around Y-123 grains, which are believed to be the main reason for the remarkably high T_c and J_c values by providing optimal oxygenation of the Y-123 grains and additional pinning centers. With respect to the fabricated impurity-free Y-123, RuO_2 addition raises the T_c^{zero} around 2–3 K under different magnetic fields. 3 times larger J_c values were achieved in the RuO_2 added sample over a wide range of applied magnetic fields, and this composition yielded the lowest normal state resistivity among the six different samples fabricated. The addition of three other different metal oxides, namely Al_2O_3, MoO_3, and TiO_2, also enhances current carrying capacity of the Y-123 sample around 1,5-3 times without any decrease on transition temperatures, which are considered to be the direct evidence for the presence of effective flux pinning centers within the sample. Furthermore, the addition of MoO_3 and TiO_2 has little effect on transition width of the Y-123, while adding Al_2O_3-cru significantly broadens the resistive transition.

References

1. M.K. Wu, J.R. Ashburn, C.J. Torng, P.H. Hor, R.L. Meng, L. Gao, Z.J. Huang, Y.Q. Wang, C.W. Chu, Phys. Rev. Lett. **58**, 908 (1987)
2. M. Tomita, M. Murakami, Nature **421**(6922), 517 (2003)
3. H.J. Bornemann, M. Sander, I.E.E.E. Trans, Appl. Supercond. **7**(2), 398 (1997)
4. M. Rotta, D.K. Namburi, Y.H. Shi, A.L. Pessoa, C.L. Carvalho, J.H. Durrell, D.A. Cardwell, R. Zadorosny, Ceram. Int. **45**(3), 3948 (2019)
5. M. Ozabaci, S. Rasekh, O. Kizilaslan, M.A. Madre, A. Sotelo, M.E. Yakinci, JOM **67**(1), 222 (2015)
6. P. Pahlke, M. Sieger, R. Ottolinger, M. Lao, M. Eisterer, A. Meledin, G.V. Tendeloo, J. Hänisch, B. Holzapfel, L. Schultz, K. Nielsch, R. Hühne, Supercond. Sci. Technol. **31**, 044007 (2018)
7. Y.A. Opata, J.F.H.L. Monteiro, A.R. Jurelo, E.C. Siqueira, Phys. C **549**, 107 (2018)
8. M. Radusovska, L. Vojtkova, S. Piovarci, M. Rajnak, P. Diko, I.E.E.E. Trans, Appl. Supercond. **28**(4), 6800904 (2018)
9. C. Li, H. Suo, S. Ye, M. Liu, L. Ma, M. Tian, Y. Wang, J. Supercond. Nov. Magn. **31**, 2705 (2018)
10. S. Dadras, S. Falahati, S. Dehghani, Phys. C **548**, 65 (2018)
11. S.V. Savich, A.V. Samoylov, S.N. Kamchatnaya, O.V. Dobrovolskiy, R.V. Vovk, A.L. Solovjov, L.V. Omelchenko, J. Mater. Sci. **28**, 11415 (2017)
12. S. Chamekh, A. Bouabellou, Y. Elerman, M. Kaya, I. Dincer, J. New Technol. Mater. **7**(2), 22 (2017)
13. F. Wang, J. Mater. Sci. **27**, 7084 (2016)
14. M. Sun, Z. Liu, C. Bai, Y. Guo, Y. Lu, F. Fan, C. Cai, Phys. C **519**, 47 (2015)
15. P. Lazic, D. Pelc, M. Pozek, V. Despoja, D.K. Sunko, J. Supercond. Nov. Magn. **28**, 1299 (2015)
16. N. Soylu, C.C. Yahsi, S.P. Altintas, S. Nezir, C. Terzioglu, J. Supercond. Nov. Magn. **26**, 1945 (2013)
17. B. Çakır, A. Aydıner, J. Mater. Sci. **28**, 17098 (2019)
18. S.H. Naqib, A. Semwal, Phys. C **425**(1–2), 14 (2005)
19. D. Volochova, V. Antal, S. Piovarci, J. Kovac, M. Jirsa, J.G. Noudem, P. Diko, I.E.E.E. Trans, Appl. Supercond. **26**(3), 7200604 (2016)
20. F. Wang, H. Tian, J. Mater. Sci. **30**, 4137 (2019)
21. R.V. Vovk, G.Y. Khadzhaia, O.V. Dobrovolskiy, Solid State Commun. **282**, 5 (2018)
22. T. Sueyoshi, T. Kotaki, Y. Uraguchi, M. Suenaga, T. Makihara, T. Fujiyoshi, N. Ishikawa, Phys. C **530**, 72 (2016)
23. C.P. Bean, Phys. Rev. Lett. **8**, 250 (1962)
24. U. Oztornaci, B. Ozkurt, Ceram. Int. **43**, 4545 (2017)
25. J. Jaroszynski, F. Hunte, L. Balicas, Y. Jo, I. Raicevic, A. Gurevich, D.C. Larbalestier, F.F. Balakirev, L. Fang, P. Cheng, Y. Jia, H.H. Wen, Phys. Rev. B **78**, 174523 (2008)
26. C-J Kim, J.S. Yoon, K. No, S.C. Han, Y.H. Han, B-H. Jun, Supercond. Sci. Technol. 23, 125009 (2010)
27. K. Rogacki, B. Dabrowski, O. Chmaissem, Phys. Rev. B **73**, 224518 (2006)
28. E. Yanmaz, S. Balci, T. Küçükömeroğlu, Mater. Lett. **54**, 191 (2002)
29. P. Diko, L. Shlyk, G. Krabbes, Phys. C **390**, 143 (2003)
30. L. Shlyk, B. Schüpp, G. Krabbes, K. Nenkov, G. Fuchs, Phys. C **406**, 107 (2004)
31. N. Moutalibi, A. Mchirgui, Phys. C **469**, 95 (2009)